ChemComm

Material Composition and Peptide Sequence Affects Biomolecule Affinity to and Selectivity for h-Boron Nitride and Graphene

Journal:	*ChemComm*
Manuscript ID	CC-COM-04-2020-002635.R1
Article Type:	Communication

COMMUNICATION

Material Composition and Peptide Sequence Affects Biomolecule Affinity to and Selectivity for *h*-Boron Nitride and Graphene

Received 00th January 20xx,
Accepted 00th January 20xx

DOI: 10.1039/x0xx00000x

Nermina Brljak,[a] Atul D. Parab,[a] Rahul Rao,[b] Joseph M. Slocik,[b] Rajesh R. Naik,[b] Marc R. Knecht,[a,c,†,*] Tiffany R. Walsh[d,†,*]

Nanosheet heterostructures offer emergent optical/electronic properties. These could be achieved using selective materials binding peptides, but lack of understanding of selectivity impedes advancement. Here we examine peptides with affinity for graphene or *h*-BN using quantitative experiments and molecular simulation to identify traits for design of 2D nanosheet selective peptides.

Two dimensional (2D) nanosheet materials have garnered extensive scientific interest due to their unique electronic and optical properties, making them ideal structures for device production.[1-4] Most studies have focused on graphene, a semimetal nanosheet, which has been exploited for a variety of electronic applications.[4] The properties of graphene arise from its molecular structure of hexagonally arrayed sp^2 carbons, giving rise to its intrinsic conductive properties. Hexagonal boron nitride (*h*-BN) possesses a very similar array of atoms in the nanosheet; however, the material is a wide band gap semiconductor (~5.9 eV), making it an electrical insulator.[2] While expansive literature has explored graphene, considerably less focus has been on *h*-BN, where studies have suggested that *h*-BN/graphene heterostructures could be important for electronic applications.[5, 6] New methods are required to efficiently generate such structures to elucidate and measure emergent properties under high throughput approaches.

While a variety of traditional methods have been identified to synthesize, exfoliate, and/or assemble nanosheets, these approaches can require caustic conditions, high temperatures, and/or laborious steps that lead to defect incorporation. As an alternative, biomimetic methods have been developed for nanomaterial synthesis and processing that use ambient conditions, which could minimize defects.[3] For instance, peptides with affinity for graphene have been identified, which form a unique bio-overlayer on the carbon surface.[7-9] These biomolecules can be used to drive graphene exfoliation from bulk graphite,[10] regiospatially incorporate Au nanoparticles on the nanosheet,[8] etc., thus delivering wide ranging capabilities.

While considerable information is known for peptides on graphene, very little knowledge of peptides with affinity for *h*-BN is available.[3, 11, 12] Hanagata and coworkers identified a library of sequences with affinity for BN nanospheres (BNNS), most notably BP1 (LLADTTHHRPWT) and BP7 (VDAQSKSYTLHD), evaluated using semi-quantitative binding assays.[12] While these sequences are anticipated to bind *h*-BN, rigorous quantification of the binding affinity (ΔG) remains unstudied. In addition, these sequences possess numerous hydrophobic/aromatic residues, which are likely to have affinity for graphene. This initial study suggested that the BP1 peptide bound both BNNS and carbon nanotubes (CNTs), while the BP7 showed selective binding for BNNS over CNTs.[12] However, these experiments, used a peptide conjugated to an aromatic dye (fluorescein-5-isothiocyanate, FITC). Since aromatic groups are anticipated to bind to graphene and interact with aromatic biomolecule contents, the dye might influence the binding (and conformational) properties of the peptides. While such studies provide intriguing initial results, the level of binding affinity and selectivity for isoelectronic nanosheets such as *h*-BN and graphene by peptides remains unclear and must be fully understood to facilitate biomimetic organization of 2D materials using label-free conditions.

In this work, we examine the affinity and selectivity of three materials binding peptides for 2D nanosheets: BP1, BP7, and P1 (HSSYWYAFNNKT). The first two are anticipated to bind to *h*-BN, while P1 was previously shown to have affinity for the basal plane of graphene.[8] All three sequences possess both hydrophobic and aromatic residues, thus providing sites for binding to the hydrophobic nanosheets. Consideration of the unbound, solution-based structure as well as the structure of

[a] *Department of Chemistry, University of Miami, 1301 Memorial Drive, Coral Gables, Florida 33146, United States.*
[b] *Air Force Research Laboratory, Wright-Patterson Air Force Base, Ohio, 45433, United States.*
[c] *Dr. J.T. Macdonald Foundation Biomedical Nanotechnology Institute, University of Miami, Miami, Florida, 33136, United States.*
[d] *Institute for Frontier Materials, Deakin University, Geelong, 3216 VIC, Australia.*
† These authors contributed equally.
Electronic Supplementary Information (ESI) available: Computational/experimental methodology, additional analysis, and discussion.See DOI: 10.1039/x0xx00000x

the peptide adsorbed to both *h*-BN and graphene was computationally assessed, while the binding affinities of the sequences were quantified using Quartz Crystal Microbalance (QCM) analysis. The results indicate that while the sequences do not demonstrate substantial material selectivity, the binding mode of the peptides were distinctly different on the two materials. This allows for unambiguous identification of the set of anchor residues to the different nanosheets providing a pathway towards the *de novo* design of new sequences with desired materials compositional selectivity.

Conformational analysis (both experimental and modelling) of the three peptides in solution indicated that random coil structures were dominant in all cases (see ESI). For the surface adsorbed states, molecular simulation can predict the degree of residue-surface contact for each sequence, adsorbed at the aqueous *h*-BN and graphene interfaces. The overall contact between a peptide and a solid surface cannot be typically characterised by the sum of each individual residue/surface interaction, owing to the complex interplay between the peptide sequence and its overall 3D structure in the adsorbed state.[13, 14] Often, materials-specific peptides are intrinsically disordered, such that the resultant types of conformations in the adsorbed state are numerous, and are best represented as a statistical ensemble. To capture this ensemble for both BP1 and BP7, Replica-Exchange with Solute Tempering Molecular Dynamics (REST-MD) simulations[15, 16] were used, along with the GRAPPA[17] and BoNi-CHARMM[18] force-fields for graphene and *h*-BN, respectively. Outcomes from the REST-MD simulation approach have demonstrated consistency with experimental data on numerous occasions for similar systems.[19-22] At present, molecular simulations of biomolecules adsorbed at aqueous *h*-BN are scarce;[3] these data provide essential insights into how these peptides engage with the surface.

The predicted residue-surface contact data, summarised for both substrates in Fig 1, indicate that for *h*-BN, aliphatic and aromatic residues in general featured the greatest contact. On graphene the dominance of aromatic-mediated contact in general appeared more pronounced, with a relatively lower degree of aliphatic contact compared with *h*-BN, albeit with some exceptions (*e.g.* Leu10 in BP7). The degree of strong contact particularly for the aromatic groups appeared to be dependent on the sequence position and local sequence environment (*i.e.* Trp11 in BP1 vs. Trp5 in P1 both on graphene).

Asp, His, Lys, and Ser are predicted to be poor binders to *h*-BN, regardless of their sequence position (Fig 1). Hanagata and coworkers reported Ala mutation binding data for seven sites in the BP7 sequence;[12] these sites are indicated by the dark grey and red coloured bars in Fig 1. The red bars indicate a mutation site that resulted in negligible change to *h*-BN binding (Asp2, Lys6, His11, Asp12). The predicted poor contact of these sites by the REST-MD simulations shows remarkable consistency with these mutation data. Similarly, the dark grey bars in Fig 1 indicate mutation sites that yielded a substantial drop in binding (Val1, Tyr8, Leu10). The predicted strong contact of these three residues (Fig 1) is consistent with the mutation data.

The overall statistics regarding the degree of contact between the entire peptide and the surface were also

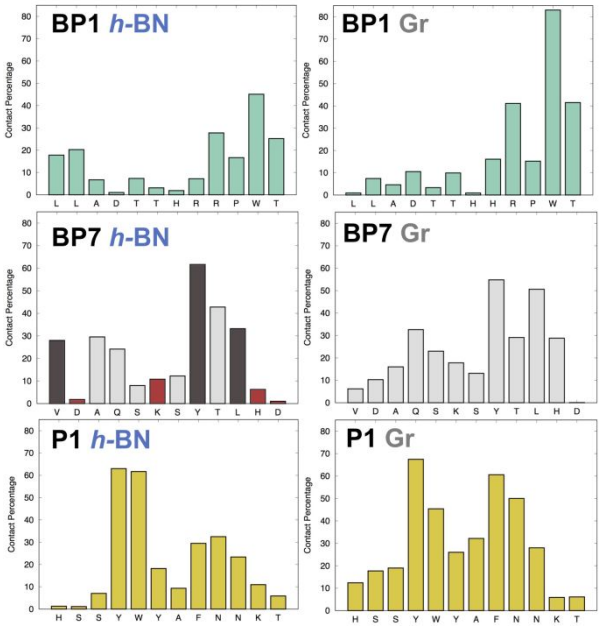

Fig 1. Quantification of residue-surface contact (expressed as a percentage of the simulation trajectory), determined from replica-exchange with solute tempering molecular dynamics simulations, for each of the three peptides, adsorbed at both aqueous *h*-BN and graphene interfaces. The dark grey and red bars shown for the BP7/*h*-BN interface indicate mutation sites (explained in main text).

quantified, in terms of the relative fraction of surface-adsorbed vs. unadsorbed states. While not strictly a measure of the binding constant, the ratio of these values is a useful guide to the peptide binding strength. To this end, on the *h*-BN surface, BP1, BP7, and P1 had an adsorbed:unadsorbed ratio of 68:32, 62:38, and 75:25, respectively. On graphene these ratios were 92:8, 93:7, and 100:0, respectively, suggestive of stronger binding on graphene over *h*-BN. On the basis of the pattern of residue-surface contact, and on these ratios, P1 is expected to be a stronger binder on *h*-BN compared with BP1 and BP7 (which are expected to be similar in binding strength). These predictions are consistent with the experimental data (discussed below). These predictions also suggest that BP1 and BP7 bind with similar strengths on both substrates, which differs from the semi-quantitative binding analysis of FITC-labelled BP7.[12] The source of this discrepancy might be due to the presence of the covalently-attached FITC dye.

In terms of structural evaluation, all peptides in the surface adsorbed state were dominated by random coil characteristics, with β-turns being the next most abundant feature, as indicated by computational secondary structure analyses (ESI, Table S2). No dramatic changes in the percentage fraction of each type of secondary structure motif were observed between the in-solution and surface-adsorbed systems, regardless of the substrate, graphene or *h*-BN (ESI, Tables S1 and S2). This finding does not agree with the circular dichroism (CD) data reported by Hanagata and coworkers, who found that the CD spectrum of BP7 adsorbed to BNNS differed with that of the in-solution spectrum.[12] This difference may be attributed to the FITC dye.

Clustering analyses, where the adsorbed ensemble is classified into groups of similar structures, can provide information in terms of the overall number of such similar structures (denoted as clusters) and their relative population in the ensemble. The most populated cluster in the surface-

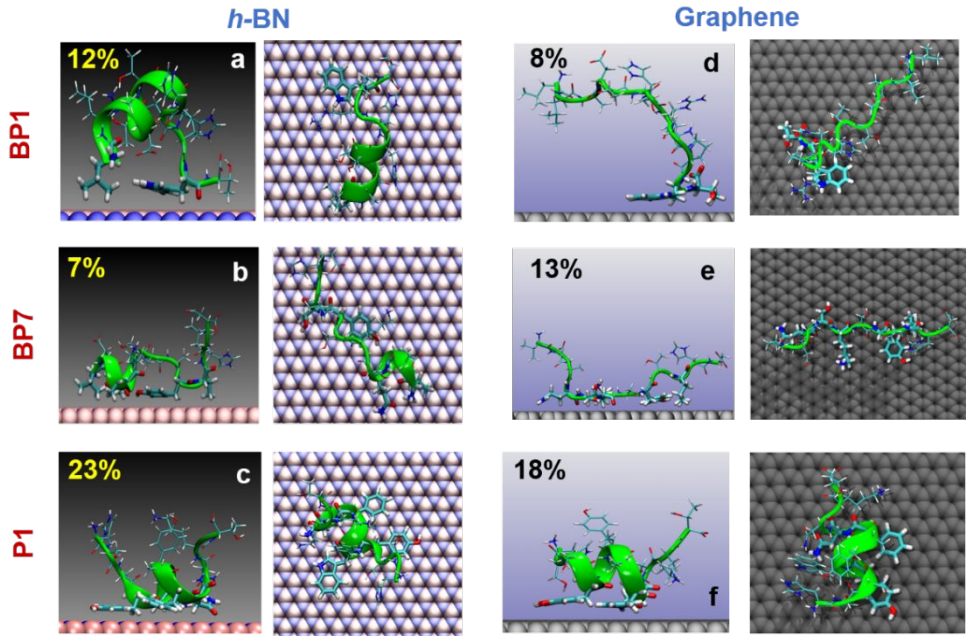

Fig. 2. Surface-adsorbed structures predicted from replica-exchange with solute tempering molecular dynamics simulations, for each of the three peptides, at both aqueous *h*-BN and graphene interfaces (water not shown for clarity). Each panel presents a representative of the most-populated cluster in both plan- and side-view, with the population fraction of this cluster indicated in the top left corner. (a and d) BP1, (b and e) BP7, (c and f) P1.

adsorbed state for each case is presented in Fig 2. All three peptides were indicated to be entropic binders,[23] characterised by high numbers of clusters (on *h*-BN/graphene: 187/169, 193/158, and 173/168 for BP1, BP7, and P1, respectively) and strongly peaked population distributions. In several, but not all, instances the most populated cluster possessed some degree of secondary structuring (Fig 2); however, as the population data indicate (ESI, Fig S4), the majority of clusters featured random coil characteristics. Although each of these has a relatively small population, collectively these vastly outnumbered the more structured conformations, contributing to the overall dominance of the random coil characteristics.

To complement the modelling analysis, experimental quantification of the affinity of the three peptides was assessed using QCM on both *h*-BN and graphene. To generate the interface, *h*-BN or graphene was deposited onto Au QCM sensors using previously described methods.[24] The nanosheet deposition process was confirmed using X-ray photoelectron (XPS) and Raman spectroscopies (ESI, Fig S5). Once the sensors were prepared, they were purified via UV ozone to remove any adsorbed materials and washed with water. To quantify the binding, various concentrations of the biomolecule were flowed over the sensor surfaces. The binding was monitored via changes in the resonant frequency where the resulting data were fit using the Langmuir isotherm. From this fitting, a k_{obs} value was determined at each concentration, where plotting of these data was used to extract information to calculate ΔG values using established approaches.[23, 25]

Fig. 3a presents the binding analysis for the BP7 peptide on *h*-BN. The data are inverted for a more intuitive interpretation. Additionally, the dissipation energy is shown, which is sufficiently small, confirming that a rigid biomolecular overlayer was generated on *h*-BN. Fig 3b compares the k_{obs} values of the binding as a function of concentration, from which the k_a and k_d constants were extracted based upon the slope and *y*-intercept of the line of best fit. Using these values, a ΔG of -29.5 ± 0.3 kJ/mol was calculated for the affinity of the BP7 on *h*-BN. From this analysis for the BP1 and P1 peptides, ΔG values of -29.6 ± 0.6 and -33.0 ± 2.2 kJ/mol, respectively, were determined.

Using the same approach for the three peptides, but with the graphene sensor surface, variations in the affinity of the peptide were observed. Previously, the affinity of the P1 peptide for graphene was reported to be -35.6 ± 2.3 kJ/mol.[26] When the graphene binding analysis was processed using BP7 and BP1, ΔG values of -33.5 ± 3.9 and -33.6 ± 0.3 kJ/mol were determined, respectively. Such values suggested enhanced binding on graphene over *h*-BN, which likely arises due to changes in the nanosheet electronic structure.

Taken together, the QCM results and the modelling studies indicate three key points for peptide binding to *h*-BN and graphene. First, the BP7 and BP1 peptides have nearly identical affinity for *h*-BN. This can also be said for graphene, but with a stronger overall binding for both. Second, regardless of the

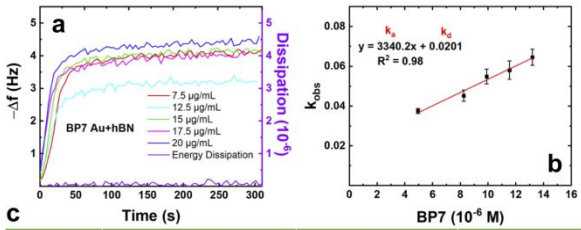

c

Peptide	Sequence	ΔG Graphene (kJ mol⁻¹)	ΔG *h*-BN (kJ mol⁻¹)
P1	HSSYWYAFNNKT	-35.6 ± 2.3	-33.0 ± 2.2
BP7	VDAQSKSYTLHD	-33.5 ± 3.9	-29.5 ± 0.3
BP1	LLADTTHHRPWT	-33.6 ± 0.3	-29.6 ± 0.6

Fig. 3. BP7 QCM binding analysis. Part (a) presents the binding analysis of the peptide on the *h*-BN modified Au sensors at selected concentrations, while part (b) displays a plot of the k_{obs} values as a function of peptide concentration. Part (c) compares the ΔG values for the peptides binding to *h*-BN and graphene.

material composition, the P1 sequence has greater affinity for the nanosheet than either BP7 or BP1. Third, the Δ*G* values for all of the biomolecules indicated stronger binding on graphene relative to *h*-BN, regardless of the material composition that the peptide was originally identified with affinity for.

While these studies do not suggest that selective binding of the peptides based upon material composition is apparent, they do provide fundamental information regarding which combination of residues might potentially confer such selectivity. For example, Leu and Val appear to be good *h*-BN binders, but do not bind as well to graphene. Conversely, Asn and Gln appear to bind better to graphene over *h*-BN. The fundamental physical reasons for this specificity remain an open question but might be due to differences in interfacial solvent structuring (discussion in ESI). Finally, aromatic residues bind strongly to both substrates, suggesting that these should be avoided to achieve material selectivity. Overall, this suggests that an aromatic-devoid sequence that is rich in Leu and Val but poor in Asn and Gln might show binding selectivity on *h*-BN over graphene, and conversely an aromatic-devoid sequence rich in Asn/Gln and poor in Leu/Val could potentially deliver binding selectivity on graphene over *h*-BN. Although the lack of aromatic content would presumably weaken the overall binding strength in both instances, a compromise on binding affinity is a typical outcome when seeking binding selectivity.

While the present results suggest that BP7 can bind both *h*-BN and graphene, Hanagata and coworkers reported selective binding of the FITC-labeled version of the sequence on BNNS over CNTs.[12] It is important to note key differences between these. For instance, this study uses label-free peptides for binding to flat 2D nanosheets. These significant variations could give rise to the differences in binding, especially considering the potential curvature of the CNTs from the prior study. The influence of fluorescent tags is a long-standing, entrenched issue in this field and its resolution is outside the scope of the current work. However, the presence of aromatic groups in the non-peptide part of the conjugate molecule has been previously shown (using both experiment and modelling) to affect both the binding strength and binding conformation of peptide conjugates on Au and Ag surfaces depending on the attachment point,[27, 28] which suggests that similar effects were possible in the FITC-label experiments. [12]

In conclusion, this work has elucidated fundamental insights that provide a pathway towards the identification of peptides with selective affinity for *h*-BN or graphene. Such capabilities could enable controlled deposition and manipulation of 2D nanosheets under ambient conditions. This could enable the bio-mediated production of 2D nanosheet heterostructures of controlled composition and arrangement under ambient conditions to realize emergent electronic and optical properties.

This material is based upon work supported by the Air Force Office of Scientific Research, Grant FA9550-18-1-0329. TRW thanks the National Computing Infrastructure (NCI), Canberra, and the Pawsey Supercomputing Facility, Perth, Australia, for computational resources provided under the NCMAS scheme.

Conflicts of interest

There are no conflicts to declare.

Notes and references

1. G. R. Bhimanapati, Z. Lin, V. Meunier, Y. Jung, J. Cha, S. Das, D. Xiao, Y. Son, M. S. Strano, V. R. Cooper, L. Liang and e. al., *ACS Nano*, 2015, **9**, 11509-11539.
2. M. Xu, T. Liang, M. Shi and H. Chen, *Chem. Rev.*, 2013, **113**, 3766-3798.
3. T. R. Walsh and M. R. Knecht, *Bioconjug. Chem.*, 2019, **30**, 2727-2750.
4. V. Georgakilas, J. N. Tiwari, K. C. Kemp, J. A. Perman, A. B. Bourlinos, K. S. Kim and R. Zboril, *Chem. Rev.*, 2016, **116**, 5464-5519.
5. F. Liu, R. Zou, N. Hu, H. Ning, C. Yan, Y. Liu, W. L., F. Mo and S. Fu, *Nanoscale*, 2019, **11**, 4067-4072.
6. L. Wang, S. Zihlmann, M.-H. Liu, P. Makk, K. Watanabe, T. Taniguchi, A. Baumgartner and C. Schönenberger, *Nano Lett.*, 2019, **19**, 2371-2376.
7. Y. Cui, S. N. Kim, S. E. Jones, L. L. Wissler, R. R. Naik and M. C. McAlpine, *Nano Lett.*, 2010, **10**, 4559-4565.
8. S. N. Kim, Z. Kuang, J. M. Slocik, S. E. Jones, Y. Cui, B. L. Farmer, M. C. McAlpine and R. R. Naik, *J. Am. Chem. Soc.*, 2011, **133**, 14480-14483.
9. C. R. So, Y. Hayamizu, H. Yazici, C. Gresswell, D. Khatayevich, C. Tamerler and M. Sarikaya, *ACS Nano*, 2012, **6**, 1648-1656.
10. A. D. Parab, A. Budi, J. M. Slocik, R. Rao, R. R. Naik, T. R. Walsh and M. R. Knecht, *J. Phys. Chem. C*, 2020, **124**, 2219-2228.
11. Z. Gao, C. Zhi, Y. Bando, D. Golberg and T. Serizawa, *J. Am. Chem. Soc.*, 2010, **132**, 4976-4977.
12. H. Zhang, T. Yamazaki, C. Zhi and N. Hanagata, *Nanoscale*, 2012, **4**, 6343-6350.
13. T. R. Walsh, *Accounts Chem Res*, 2017, **50**, 1617-1624.
14. T. R. Walsh and M. R. Knecht, *Chem Rev*, 2017, **117**, 12641-12704.
15. L. B. Wright and T. R. Walsh, *Phys. Chem. Chem. Phys.*, 2013, **15**, 4715-4726.
16. T. Terakawa, T. Kameda and S. Takada, *J. Comput. Chem.*, 2011, **32**, 1228-1234.
17. Z. E. Hughes, S. M. Tomasio and T. R. Walsh, *Nanoscale*, 2014, **6**, 5438-5448.
18. A. Budi and T. R. Walsh, *Langmuir*, 2019, **35**, 16234-16243.
19. S. Mokashi-Punekar, T. R. Walsh and N. L. Rosi, *J. Am. Chem. Soc.*, 2019, **141**, 15710-15716.
20. L. B. Wright, J. P. Palafox-Hernandez, P. M. Rodger, S. Corni and T. R. Walsh, *Chem. Sci.*, 2015, **6**, 5204-5214.
21. Z. E. Hughes and T. R. Walsh, *Nanoscale*, 2018, **10**, 302-311.
22. A. M. Sultan, Z. C. Westcott, Z. E. Hughes, J. P. Palafox-Hernandez, T. Giesa, V. Puddu, M. J. Buehler, C. C. Perry and T. R. Walsh, *ACS Appl. Mater. Interfaces*, 2016, **8**, 18620-18630.
23. Z. Tang, J. P. Palafox-Hernandez, W.-C. Law, Z. E. Hughes, M. T. Swihart, P. N. Prasad, M. R. Knecht and T. R. Walsh, *ACS Nano*, 2013, **7**, 9632-9646.
24. S. S. Kim, Z. Kuang, Y. H. Ngo, B. L. Farmer and R. R. Naik, *ACS Appl. Mater. Interfaces*, 2015, **7**, 20447-20453.
25. C. Tamerler, E. E. Oren, M. Duman, E. Venkatasubramanian and M. Sarikaya, *Langmuir*, 2006, **22**, 7712-7718.
26. A. D. Parab, A. Budi, N. Brljak, M. R. Knecht and T. R. Walsh, 2020, submitted.
27. J. P. Palafox-Hernandez, C.-K. Lim, Z. Tang, K. L. M. Drew, Z. E. Hughes, Y. Li, M. T. Swihart, P. N. Prasad, M. R. Knecht and T. R. Walsh, *ACS Appl. Mater. Interfaces*, 2016, **8**, 1050-1060.
28. Z. Tang, C.-K. Lim, J. P. Palafox-Hernandez, K. L. M. Drew, Y. Li, M. T. Swihart, P. N. Prasad, T. R. Walsh and M. R. Knecht, *Nanoscale*, 2015, **7**, 13638.